International Information and Engineering Technology Association
Advancing the World of Information and Engineering

International Journal of Heat and Technology
Vol. 42, No. 5, October, 2024, pp. 1727-1734
Journal homepage: http://iieta.org/journals/ijht

Thermal Stress Simulation of Motor-Control Circuit Boards Using Finite Angle Motors: Heat Dissipation and Structural Optimization Through COMSOL Coupling Analysis

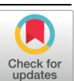

Yuanwei Zheng[1], Anjiang Lu[2*], Hua Zhou[2], Jiao Yang[2]

[1] Information Center of Guizhou Power Grid Company Ltd, Guiyang 550002, China
[2] College of Big Data and Information Engineering, Guizhou University, Guiyang 550025, China

Corresponding Author Email: ajlu@gzu.edu.cn

Copyright: ©2024 The authors. This article is published by IIETA and is licensed under the CC BY 4.0 license (http://creativecommons.org/licenses/by/4.0/).

https://doi.org/10.18280/ijht.420527

Received: 12 April 2024
Revised: 25 August 2024
Accepted: 19 September 2024
Available online: 31 October 2024

Keywords:
heat flux density, 3D modelling, COMSOL finite element simulation, thermal stress, heat dissipation optimization

ABSTRACT

To accelerate the transition from design to production and enhance the reliability of motor-control circuit boards, a coupling simulation analysis of thermal stress and heat transfer has been conducted using COMSOL Multiphysics software. The investigation focuses on the thermal performance of the circuit board at 85℃, examining the effects of copper layer thickness on heat dissipation. The influence of heat dissipation through-holes on thermal management was also explored to determine optimal design parameters. A systematic approach was adopted to optimize copper skin thickness and through-hole configurations, with the goal of minimizing thermal stress and deformation displacement. COMSOL was employed to validate the effectiveness of the proposed cooling scheme. The simulation results indicate that the optimized design reduces average temperature by 9.86%, mitigates thermal stress by 10.47%, and lowers deformation displacement by 22.4%, confirming the feasibility of the thermal management strategy. These findings offer practical insights into the structural layout and lamination design of motor-control circuit boards, with implications for improving product development efficiency and reliability.

1. INTRODUCTION

Nowadays, due to the gradual development of electronic equipment towards miniaturization and integration, the heat flux density of electronic equipment increases rapidly, and the heat dissipation design of electronic equipment restricts the development of electronic product technology to a large extent [1-8]. Studies have shown that among the environmental factors such as temperature, humidity, vibration, and dust that cause electronic equipment failure, temperature accounts for 55% of the proportion [9-11]. And as the temperature increases, the failure probability value of components shows an exponential growth trend. For every 10℃ increases in temperature, the failure rate doubles, which is called the 10℃ rule. At present, due to the development of environmental temperature and electronic equipment in a more highly integrated direction, the heat generated by electronic equipment during operation cannot be transmitted in a timely and efficient manner, resulting in a rapid increase in the temperature of electronic components, which may cause PCB deformation to lead to electronic components falling off or causing damage. And the temperature of electronic components increases rapidly, which may also make the working performance of electronic components deteriorate or even burn out in diameter. The appearance of these possible situations will seriously affect the reliable performance of electronic equipment [12-20]. In order to address the actual needs of the current heat dissipation design of electronic equipment, many researchers use computer simulation technology to conduct heat dissipation simulation design for electronic equipment, and use temperature measurement technology to measure the temperature of the heat dissipation optimized entity of their electronic equipment, verifying the effectiveness of the heat dissipation design scheme. Thornton and Dechaumphai [21] used Full Coupling to analyze the computational domain of multi-physics coupling simulations such as heat transfer field, solid mechanics field, and flow field. In literature [22], the COMSOL simulation software was used to study the temperature distribution and thermal stress distribution of a small heating circuit board, and the most prone to failure area of the circuit board was obtained, and it was found that the thermal stress was the largest at the inner corner of the circuit curve, and reduce the effective stress and deflection of the circuit board by reducing the thickness of the substrate. For every 1um increase in the thickness of the substrate, the effective stress will increase by 2MPa, and the improvement will double, and the deflection will increase by 5um, an improvement of 50%.

In this study, the finite-angle motor control circuit board is selected as the research object, and a three-dimensional simulation model of its components and PCB is developed. Based on the principles of heat transfer, the thermal simulation software COMSOL is utilized to perform coupled simulations involving heat transfer, stress, and other multiphysics fields. The simulations yield the distribution of key physical parameters, including temperature, stress, and deformation displacement.

2. LIMITED ANGLE MOTOR CONTROL BOARD

The limited-angle motor control circuit board consists of an upper and a lower control circuit board. The upper control circuit board primarily contains a low-power control module composed of chips for signal processing. In contrast, the lower control circuit board houses high-power components, including high-power Schottky diodes, MOSFETs, and power conversion modules. An external metal enclosure is used to secure the control circuit board, assist in heat dissipation, and mount the assembly onto the gas turbine control system. The structural design of the finite-angle motor controller is illustrated in Figure 1.

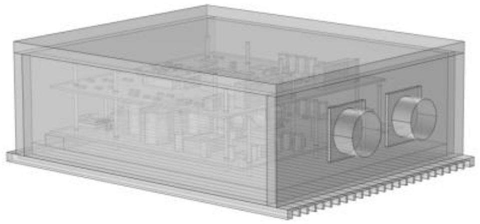

Figure 1. Controller structure diagram of finite angle motor

On the lower control circuit board, power consumption is significantly high due to the presence of the power supply circuit and the motor H-bridge drive circuit, resulting in a high heat flux density. Instead of relying on conventional experience-based methods for thermal stress design, COMSOL is employed to simulate the thermal stress of the lower control circuit board, optimizing its thermal performance. This approach not only shortens the development cycle but also enhances the controller's precision.

3. MULTIPHYSICS SIMULATION ANALYSIS

The COMSOL finite element simulation of the controller and the lower control circuit board primarily follows the steps outlined in Figure 2. It mainly includes the establishment of a simulation model and model simplification, physical field addition and boundary condition setting, multi-physics interface setting, material definition, meshing, solver setting and simulation solution, post-processing, and other main processes.

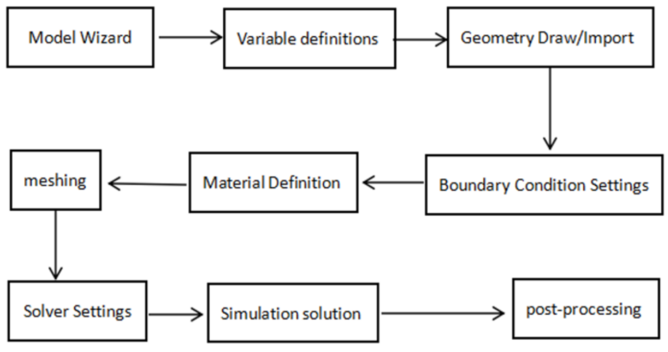

Figure 2. Finite element simulation step diagram

Establishing the 3D simulation model of the control circuit board involves creating models of electronic components and PCB boards, among other elements. It is mainly modeled and designed in the SoildWorks software according to the dimensions of the relevant modules and the data manuals, then assembled in the SoildWorks software, and finally imported into COMSOL using the LiveLink interface in the COMSOL software. The three-dimensional simulation model of the lower control circuit board is shown in Figure 3.

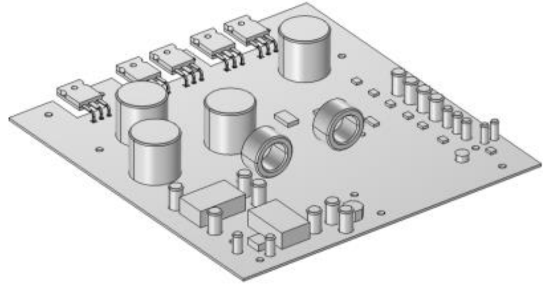

Figure 3. 3D simulation model of the control circuit board

The lower control circuit board has two physical fields of solid heat transfer and solid mechanics. By analyzing the principle of hardware circuit design and the data of related electronic components, we have calculated the power consumption of electronic components with high power, as shown in Table 1.

Table 1. Power consumption of electronic components related to the control circuit board

Component Model	Power Consumption / W
Diode	1.47
MOSFET	3.692
24 V to ± 12 V	0.7459
24 V to 5 V	0.6818
5 V to 3.3 V	1.02
HIP4080	0.47
LM158	0.55
INA114	0.1
HC02	0.12
HC74	0.105
LM2903	0.57
TL082I	0.68

For the multiphysics coupled simulation of the control circuit board, the ambient temperature is set to the industrial control maximum of 85℃, with heat transfer by thermal radiation neglected. The heat transfer coefficient between the simulation entity and the external environment is set to 3 W/(m² K). The power consumption of the power components on the control circuit board is treated as the heat source. The circuit board's mounting holes are assigned as fixed constraints. Based on Table 1 and the relevant boundary conditions, initial values, heat flux, thermal insulation, gravity direction, and other parameters are configured, with the multiphysics field set to thermal expansion.

According to the materials used in the simulation model of the lower control circuit board, relevant material properties are added and configured within COMSOL. The material properties of each component are detailed in Table 2.

Since the circuit board is laminated by copper skin, prepreg (PP sheet), and epoxy glass cloth (FR-4), and the thickness of copper skin and prepreg is relatively small compared to the thickness of epoxy glass cloth, it can be negligible. Therefore, the heat transfer coefficient of the circuit board in the thickness direction is equal to the heat transfer coefficient of FR-4, namely: $k_z = k_{FR-4} = 0.3\mathrm{W/(m \cdot K)}$; but, in the plane

direction of the circuit board, due to the influence of the copper area, the equivalent thermal conductivity in the plane direction can be obtained by Eq. (1):

$$k_x = k_y = k_{Cu} \cdot v_{Cu} + k_{FR-4} \cdot (1 - v_{Cu}) \quad (1)$$

Table 2. Material properties of simulation model of control circuit board

Material	Thermal Conductivity/W/(m·K)	Specific Heat/J/(kg·K)	Density/Kg/m^3	Young's Modulus/Pa	Poisson's Ratio	Thermal Expansion Coefficient/1/K
Copper	400	385	8960	1.1×10^{11}	0.35	1.7×10^{-5}
Epoxy molding compound	0.67	500	1200	7×10^{9}	0.39	3.65×10^{-8}
Silicon	130	700	2329	1.7×10^{11}	0.28	2.6×10^{-6}
Encapsulation plastic	0.2	2700	900	3.2×10^{9}	0.22	7×10^{-5}
Aluminum package	238	900	2700	7×10^{10}	0.33	2.3×10^{-5}
Steel AISI 4340	44.5	475	7850	2.05×10^{11}	0.28	1.23×10^{-7}

In the formula: k_x and k_y are the thermal conductivity in the horizontal direction of the circuit board; k_{Cu} is the thermal conductivity of the copper sheet 400 W/(m·K); K_{FR-4} is the thermal conductivity of the epoxy glass cloth base 0.3 W/(m·K); v_{Cu} is the volume ratio of the copper content in the control circuit board.

From Eq. (1), we can see that the thermal conductivity of the control circuit board in the horizontal direction is affected by the volume ratio of copper skin. The length of the lower control circuit board is 212.5 mm and the width is 223 mm. The width of the three rectangular slots on the side is 23.38 mm, and the lengths from left to right are 21.8 mm, 44.15 mm, and 44.4 8 mm, respectively. Therefore, according to Eq. (1) and the lower circuit board in the order of signal layer, ground layer, signal layer, power layer, ground layer, and signal layer, and ignoring the mounting holes and wiring holes on the board, we can calculate the thermal conductivity of the lower control circuit board in the horizontal direction under the conditions of copper thickness of 1/8 OZ, 1/4 OZ, 1/3 OZ, 1/2 OZ, 1 OZ, 2 OZ, and 3 OZ, respectively: 3.6725, 7.0449, 9.2933, 13.7899, 27.2798, 54.2595 and 81.2393.

Next, mesh the simulation model of the lower control circuit board: Generally speaking, the greater the number of grids, the more accurate the calculation results will be. However, as the number of grids increases, it also increases the efficiency of the solution and consumes more memory. Therefore, selecting the appropriate number of grids, grid cell type, and size will greatly affect the computer requirements, solution efficiency, and solution accuracy. Generally, for complex three-dimensional simulation entities, as long as the average element quality is above 0.1, the results of the physics solution will have good convergence and the calculation results will be more accurate.

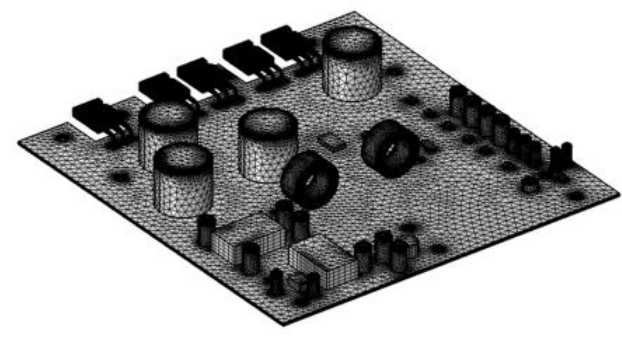

Figure 4. Control circuit board grid division diagram

After meshing, set the simulation solver. In the heat transfer-stress coupling simulation of the lower control circuit board, the simulation solver is set to the discrete step coupling solution method of the solid heat transfer physics and the solid mechanics physics field in the steady state. The simulation model of the lower control circuit board after meshing is shown in Figure 4.

Based on the above conditions, the mesh configuration was refined by adjusting parameters under the mesh size settings. Key parameters, including maximum element size, minimum element size, maximum element growth rate, curvature factor, and narrow region resolution, were fine-tuned to ensure an optimal number and quality of mesh elements. The resulting mesh statistics for the lower control circuit board are summarized in Table 3, which provides detailed information on the unit grid configuration.

Table 3. Statistical table of grid information of control circuit board unit

Items of Statistics		Quantity
Full mesh	Mesh vertex	192073
Unit type	Tetrahedron	542155
	Pyramid	600
	Prism	113901
	Triangle	189745
	Quadrilateral	11345
	Edge unit	20848
	Vertex unit	1350
Domain unit	Number of units	656656
	Minimum unit mass	0.05441
	Average unit mass	0.6838
	Unit volume ratio	3.425×10^{-6}
	Mesh volume	192800 mm^3

A thermal-stress coupling simulation was performed on the lower control circuit board using the 3D simulation model. By continuously adjusting the solver settings, improved convergence of the simulation results was achieved. Additionally, the thermal conductivity of the PCB's horizontal plane was modified iteratively. As a result, temperature distribution cloud maps, stress cloud maps, and displacement cloud maps were generated for the lower control circuit board with copper thicknesses of 1/8 OZ, 1/4 OZ, 1/3 OZ, 1/2 OZ, 1 OZ, 2 OZ, and 3 OZ. The corresponding graphs are presented in Figures 5-7.

After comparing the simulation data of different copper thicknesses, observe the maximum temperature, maximum stress, and maximum deformation displacement of the domain

of each chip under the same ambient temperature and different copper thicknesses to obtain the temperature of the same chip under the same ambient temperature and different copper thicknesses, stress, deformation, and displacement change diagram, as shown in Figure 8.

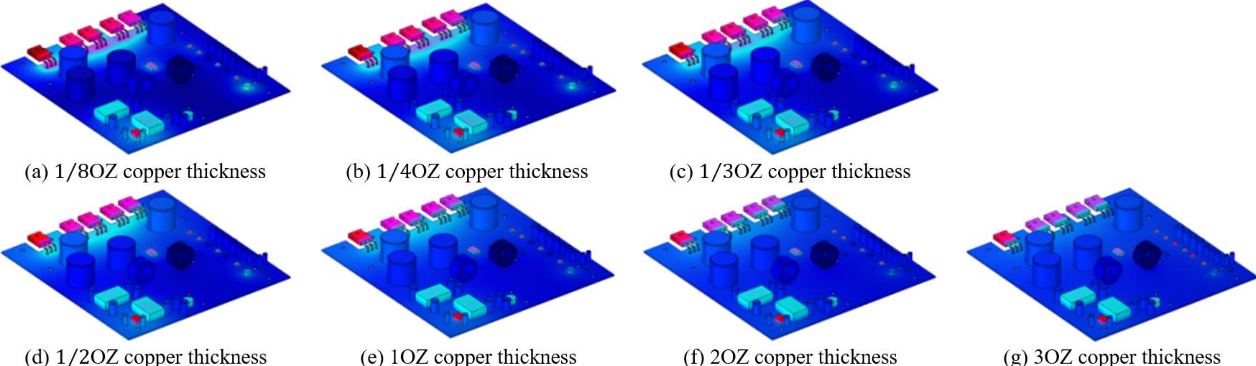

(a) 1/8OZ copper thickness (b) 1/4OZ copper thickness (c) 1/3OZ copper thickness

(d) 1/2OZ copper thickness (e) 1OZ copper thickness (f) 2OZ copper thickness (g) 3OZ copper thickness

Figure 5. Simulation temperature distribution cloud diagram of circuit board with different copper thickness

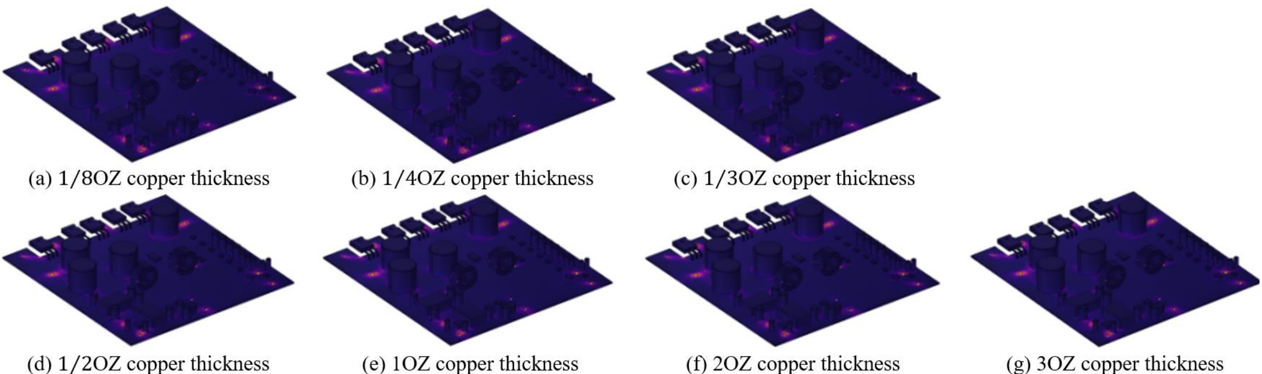

(a) 1/8OZ copper thickness (b) 1/4OZ copper thickness (c) 1/3OZ copper thickness

(d) 1/2OZ copper thickness (e) 1OZ copper thickness (f) 2OZ copper thickness (g) 3OZ copper thickness

Figure 6. Simulated stress distribution cloud diagram of circuit boards with different copper thicknesses

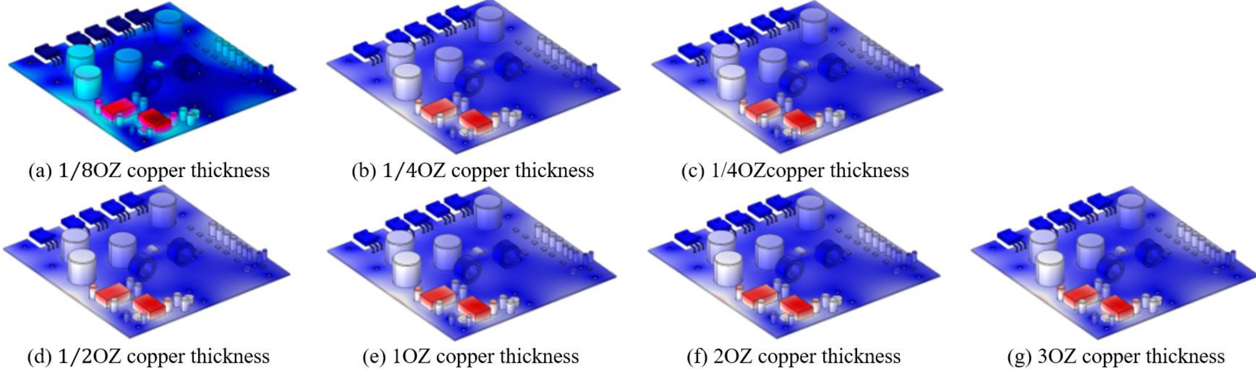

(a) 1/8OZ copper thickness (b) 1/4OZ copper thickness (c) 1/4OZcopper thickness

(d) 1/2OZ copper thickness (e) 1OZ copper thickness (f) 2OZ copper thickness (g) 3OZ copper thickness

Figure 7. Simulated displacement distribution cloud diagram of circuit boards with different copper thicknesses

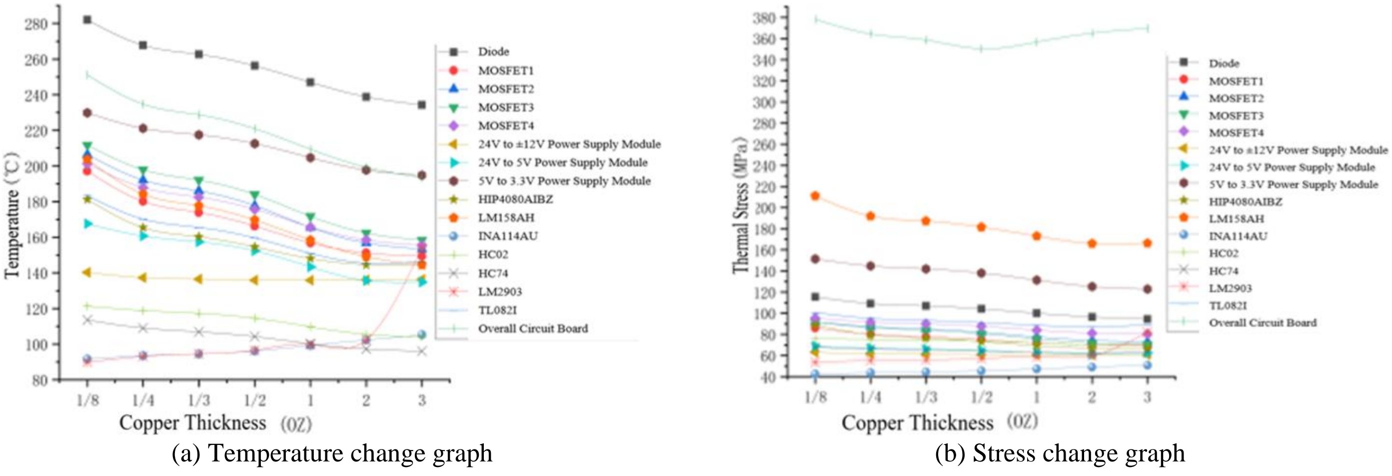

(a) Temperature change graph (b) Stress change graph

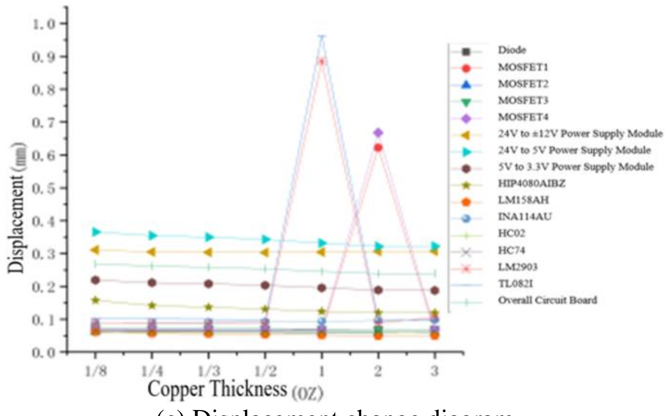

(c) Displacement change diagram

Figure 8. Temperature, stress and displacement of components under different copper thicknesses

Figure 8 clearly illustrates the significant impact of copper skin thickness on heat transfer within the circuit board. As the copper thickness increases, the temperature of most electronic components decreases; however, a small number of components experience a rise in temperature due to the baking effect. Additionally, it can be observed that the unit cooling rate within the range where the copper thickness increases from 0 OZ to 1 OZ is significantly higher than the unit cooling rate within the range where the thickness increases from 1 OZ to 3 OZ. This indicates that the cooling rate decreases with increasing copper thickness. Considering that a copper thickness of 1 OZ is commonly used in practical circuit board production and serves as the threshold for cooling rates among the seven tested thicknesses, it is determined that a copper thickness of 1 OZ should be selected for the control circuit board. Furthermore, as shown in Figures 5-7, there is little variation in the distribution of thermal stress and displacement. The thermal stress is notably greater around the fixed constraints at the mounting holes compared to other areas, and regions with higher temperatures exhibit more significant thermal deformation.

As shown from Figure 8, when the thickness of the copper skin increases, the thermal conductivity of the circuit board is gradually enhanced, and the thermal stress and deformation displacement of most of the electronic components are gradually reduced, but a small number of electronic components cause their deformation and displacement to increase because their packaging materials are aluminum or the components are located near the mounting holes. Under the thickness of 1 OZ copper skin, the maximum thermal stress of the component LM158AH is 173.14 MPa, and the maximum deformation displacement of the component TLO82I is 0.9616 mm. Based on the overall thermal stress change curve and deformation displacement change curve, as the thickness of the copper skin increases, the overall reliability of the control circuit board is getting better and better. When the thickness of the copper skin is 3 OZ, its reliability can reach the best.

Although the use of 1 OZ copper thickness on the circuit board can effectively increase the thermal conductivity of the circuit board, the temperature of some electronic components is still higher than the junction temperature of the electronic components. When operating in an environment of 85℃, the reliability of the control circuit board will be reduced, and the control circuit board may even be damaged. Therefore, it is still necessary to continue to strengthen the heat dissipation of the lower control circuit board of the motor. For optimizing the heat dissipation of the circuit board, the main methods to achieve it are to reduce its heat transfer resistance and increase the heat dissipation area; Therefore, for the optimization of heat dissipation of the lower control circuit board, on the premise of not affecting the normal operation of the circuit, we increase the heat dissipation area of the circuit board by laying a copper sheet with a thickness of 1 OZ on the bottom of the components with large heat and the bottom layer of the circuit board. At the same time, heat dissipation is optimized by connecting the copper skin at the bottom of the component to the copper skin at the bottom of the circuit board by using a 1 mm diameter thermal via to reduce the heat transfer resistance. Figure 9 shows the thermal-stress coupling simulation results at an ambient temperature of 85℃ after the heat dissipation optimization of the lower control circuit board. From left to right in the figure are the heat transfer cloud map, the stress cloud map, and the displacement cloud map.

By simulating and comparing the heat dissipation before and after optimization of the lower control circuit board, Tables 4-6 detail the changes in temperature, stress, and displacement. The simulations used a copper thickness of 1 OZ and an ambient temperature of 85℃.

Table 4. Comparison of temperature simulation results of control circuit board before and after optimization

	Temperature / ℃		
	Before Optimization	**Optimized**	**Optimization Percentage**
Diode	246.95	168.56	**31.74%**
MOSFET1	156.79	148.24	5.45%
MOSFET2	165.53	148.97	10.00%
MOSFET3	171.76	148.32	13.65%
MOSFET4	165.76	146.3	11.74%
24V to ± 12V	135.84	128.82	5.17%
24 V to 5 V	143.33	127.23	11.23%
5 V to 3.3 V	204.69	158.54	22.55%
HIP4080	148.06	106.54	28.04%
LM158	158.37	108.21	31.67%
INA114	99.282	108.88	-9.67%
HC02	109.79	105.58	3.83%
HC74	100.2	107.56	-7.35%
LM2903	99.79	149.4	-49.71%
TL082I	151.03	142.61	5.58%
Circuit board	209.45	117.67	43.82%

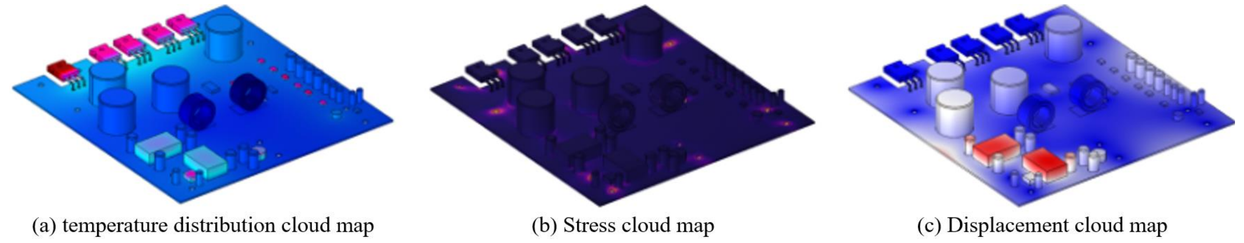

Figure 9. Simulation results of heat transfer and stress coupling after heat dissipation optimization of control circuit board

Table 5. Comparison of stress simulation results of control circuit board before and after optimization

	Thermal Stress / MPa		
	Before Optimization	**Optimized**	**Optimization Percentage**
Diode	100.07	69.933	30.12%
MOSFET1	71.821	63.649	11.38%
MOSFET2	77.656	64.939	16.38%
MOSFET3	75.661	62.495	17.40%
MOSFET4	84.082	74.983	10.82%
24V to ± 12 V	60.762	63.485	-4.48%
24 V to 5 V	62.85	64.885	-3.24%
5 V to 3.3 V	131.42	85.179	**35.19%**
HIP4080	69.218	57.024	17.62%
LM158	173.14	166.9	3.60%
INA114	47.357	57.502	-21.42%
HC02	71.86	61.715	14.12%
HC74	62.961	60.875	3.31%
LM2903	58.748	85.997	-46.38%
TL082I	88.649	94.913	-7.07%
Circuit board	356.58	35.073	90.16%

Table 6. Comparison of displacement simulation results of control circuit board before and after optimization

	Deformation Displacement / mm		
	Before Optimization	**Optimized**	**Optimization Percentage**
Diode	0.068729	0.05778	15.93%
MOSFET1	0.062793	0.061011	2.84%
MOSFET2	0.060356	0.057487	4.75%
MOSFET3	0.069938	0.065834	5.87%
MOSFET4	0.067478	0.065783	2.51%
24 V to ± 12 V	0.30454	0.28278	7.15%
24 V to 5 V	0.33153	0.30745	7.26%
5 V to 3.3 V	0.1956	0.16425	16.03%
HIP4080	0.12391	0.083897	32.29%
LM158	0.051569	0.041383	19.75%
INA114	0.093631	0.098784	-5.50%
HC02	0.059232	0.06044	-2.04%
HC74	0.062708	0.064906	-3.51%
LM2903	0.88616	0.10638	88.00%
TL082I	0.9616	0.1	**89.60%**
Circuit board	0.24573	0.055197	77.54%

The results show a substantial improvement in cooling, with a maximum temperature reduction of 31.74%. Stress and displacement also decreased significantly, by up to 35.19% and 89.60%, respectively. Although thermal conductivity enhancements led to a slight temperature increase in some components, all components' temperatures stayed below their critical junction temperatures, ensuring their reliability and preventing heat-related damage.

4. CONCLUSION

In this study, COMSOL finite element simulation software was employed to conduct a coupled heat transfer-stress analysis of the control circuit board within a finite-angle motor system. The results indicate that the thickness of the PCB's copper layer significantly influences both heat transfer and stress distribution across the board. A copper thickness of 1 OZ was selected as the optimal configuration. To further enhance thermal management, heat dissipation was improved by increasing the effective heat conduction area and minimizing thermal resistance across the board. The simulation outcomes demonstrate that the temperature, stress, and displacement were optimized by 43.82%, 90.16%, and 77.54%, respectively.

These findings validate that the proposed optimization approach can effectively enhance heat dissipation and reduce mechanical stress within the control circuit board, thereby accelerating the development process while lowering associated costs. Furthermore, the applied method provides

valuable insight for circuit board design by ensuring operational reliability under demanding thermal conditions. Although the current simulation framework offers substantial improvements, it is acknowledged that, with access to greater computational resources, more detailed simulation models could be developed in future research to further improve accuracy.

The significance of this study lies not only in the practical improvements achieved but also in the potential to extend these methodologies to more complex systems. Optimizing thermal and mechanical performance simultaneously is essential in high-power control systems, particularly where precise motor control and component reliability are critical. The insights gained from this research contribute to the development of more efficient control circuit boards, which are crucial for reducing thermal stress-induced failures and enhancing product lifespan in industrial applications.

ACKNOWLEDGMENT

This paper was supported by the Guizhou Province Natural Science Foundation (Grant No.: Qiankehe Fundamentals – ZK [2023] General-055) and Guizhou Province science and technology support plan project (Grant No.: Qiankehe Fundamentals [2023] General-465).

REFERENCES

[1] Huang, D.G., Yang, S.G. (2006). Cooling technique for high flux electronic. Fluid Machinery, 34(9): 71-74. https://doi.org/10.3969/j.issn.1005-0329.2006.09.021

[2] Liu, X., Tang, S., Feng, M. (2019). Heat dissipation analysis of electronic equipment based on CFD. Journal of Physics: Conference Series, 1300(1): 012112. https://doi.org/10.1088/1742-6596/1300/1/012112

[3] Yang, D., Yao, Q., Jia, M., Wang, J., Zhang, L., Xu, Y., Qu, X. (2021). Application analysis of efficient heat dissipation of electronic equipment based on flexible nanocomposites. Energy and Built Environment, 2(2): 157-166. https://doi.org/10.1016/j.enbenv.2020.07.008

[4] Li, R., Zhang, J. (2022). Real-time heat dissipation model of electronic equipment for determining the dynamic cooling demand of office buildings. Journal of Building Engineering, 45: 103465. https://doi.org/10.1016/j.jobe.2021.103465

[5] Jiang, S., Chen, K., Cai, Y., Tian, X. (2024). Integrated heat dissipation mechanism design of electronic equipment cabinet based on flow and sound analysis. Journal of Physics: Conference Series, 2756(1): 012047. https://doi.org/10.1088/1742-6596/2756/1/012047

[6] Garud, K.S., Lee, M.Y. (2024). Heat transfer and economic characteristics of direct oil cooling for electric traction motor under driving cycles. Applied Thermal Engineering, 258(A): 124608. https://doi.org/10.1016/j.applthermaleng.2024.124608

[7] Apalowo, R.K., Abas, A., Salim, M.R., Sharif, M.F.M., Kok, C.S. (2025). Investigating the impacts of heat sink design parameters on heat dissipation performance of semiconductor packages. International Journal of Thermal Sciences, 208: 109490. https://doi.org/10.1016/j.ijthermalsci.2024.109490

[8] Tsai, C.C., Lin, S.C., Huang, H.C., Cheng, Y.M. (2009). Design and control of a brushless DC limited-angle torque motor with its application to fuel control of small-scale gas turbine engines. Mechatronics, 19(1): 29-41. https://doi.org/10.1016/j.mechatronics.2008.07.003

[9] Wu, C. (2003). Analysis on failure of vessel electronic equipment. Journal of Wuhan University of Technology (Transportation Science & Engineering), 27(6): 796-798. https://doi.org/10.3963/j.issn.2095-3844.2003.06.015

[10] Chen, Y.X., Wang, Z.Z., Cai, Z.Y., Xiang, H.C., Wang, L.L. (2021). Adaptive prediction of remaining useful lifetime for the airborne electronic equipment based on the EM-EKF algorithm and hidden degradation model with the proportion relationship. Acta Electronica Sinica, 49(3): 500-509. https://doi.org/10.12263/DZXB.20200050

[11] Hassan, F., Hussain, A., Jamil, F., Arshad, A., Ali, H.M. (2022). Passive cooling analysis of an electronic chipset using nanoparticles and metal-foam composite PCM: An experimental study. Energies, 15(22): 8746. https://doi.org/10.3390/en15228746

[12] Mahmoud, E.E., Algehyne, E.A., Alqarni, M.M., Afzal, A., Ibrahim, M. (2022). Investigating the thermal efficiency and pressure drop of a nanofluid within a micro heat sink with a new circular design used to cool electronic equipment. Chemical Engineering Communications, 209(8): 1035-1047. https://doi.org/10.1080/00986445.2021.1935254

[13] Mutalikdesai, S.V., Kate, A.M., Shinde, T.R., Kumar Gupta, N., et al. (2023). Experimental investigation of heat transfer characteristics of inclined aluminium two phase closed thermosyphon. Kerntechnik, 88(6): 632-641. https://doi.org/10.1515/kern-2023-0045

[14] Ulman, K., Maroufi, S., Bhattacharyya, S., Sahajwalla, V. (2018). Thermal transformation of printed circuit boards at 500°C for synthesis of a copper-based product. Journal of Cleaner Production, 198: 1485-1493. https://doi.org/10.1016/j.jclepro.2018.07.140

[15] Wu, J., Yao, S., Zhao, Z., Xiao, Q., Ke, Z., Lin, Y. (2020). Thermal stress analysis of printed circuit heat exchanger based on thermal-structural coupling method. IOP Conference Series: Materials Science and Engineering, 721(1): 012034. https://doi.org/10.1088/1757-899X/721/1/012034

[16] Hu, C., Zheng, W., Zhao, B., Fan, Y., Li, H., Zheng, K., Wang, G. (2022). The effect of thermal and moisture stress on insulation deterioration law of ionic contaminated high-voltage printed circuit board of electronic power conditioner. Energies, 15(24): 9616. https://doi.org/10.3390/en15249616

[17] Pandere, V., Gautam, A., Gautam, S. (2023). A kinetic study of thermal degradation of non-metallic part of printed circuit boards for the combined effect of particle size and catalyst. Indian Chemical Engineer, 65(2): 114-124. https://doi.org/10.1080/00194506.2022.2126333

[18] Zhou, Z., Chen, J., Yu, C., Wang, Y., Zhang, Y. (2023). Failure analysis of printed circuit board solder joint under thermal shock. Coatings, 13(3): 572. https://doi.org/10.3390/coatings13030572

[19] Wan, Y., Huang, H. (2023). Thermal performance analysis and prediction of printed circuit boards. Journal of Circuits, Systems and Computers, 32(13): 2350225. https://doi.org/10.1142/S0218126623502250

[20] Perin, P., Girard, G., Martiny, M., Mercier, S. (2024). Numerical investigation of printed circuit board response

during solder float test: Influence of thermal boundary conditions. Microelectronics Reliability, 159: 115441. https://doi.org/10.1016/j.microrel.2024.115441
[21] Thornton, E.A., Dechaumphai, P. (1988). Coupled flow, thermal, and structural analysis of aerodynamically heated panels. Journal of Aircraft, 25(11): 1052-1059. https://doi.org/10.2514/3.45702
[22] Kandlikar, S.G., Ganguly, A. (2017). Fundamentals of heat dissipation in 3D IC packaging. In 3D Microelectronic Packaging: From Fundamentals to Applications. Springer, Cham, pp. 245-260. https://doi.org/10.1007/978-3-319-44586-1_10